

Supplementary Information

Amphiphilized Poly(ethyleneimine) Nanoparticles: A Versatile Multi-Cargo Carrier with Enhanced Tumor-Homing Efficiency and Biocompatibility

Solji Park,^{a,b,†} Keunsoo Jeong,^{a,c,†} Eunjung Lee,^{a,†} Jae Hyuk Lee,^b Ji Young Yhee,^a Ajay Singh,^{a,d} Joonseok Koh,^d Sangyoun Lee,^a Kwangmeyung Kim,^a Ick Chan Kwon,^a Chong Rae Park,^c Jungahn Kim,^{b,*} Sehoon Kim^{a,*}

^aCenter for Theragnosis, Korea Institute of Science and Technology, 39-1 Hawolgok-dong, Seongbuk-gu, Seoul 136-791, Korea

^bDepartment of Chemistry, Kyung Hee University, Dongdaemoon-gu, Seoul 130-701, Korea

^cCarbon Nanomaterials Design Laboratory, Global Research Laboratory and Department of Materials Science and Engineering, Seoul National University, Seoul 151-744, Korea

^dDepartment of Textile Engineering, Konkuk University, Seoul 143-701, Korea

Table S1. Molecular weights of aPEIs determine by ¹H-NMR spectrometry

	bPEI	aPEI-0	aPEI-6.3	aPEI-25
N_{C18}^1	-	5.2	5.2	5.2
N_{PEG}^1	-	-	1.9	7.7
MW (kDa)	1.8	3.1	12.6	41.6

¹ Number of conjugated octadecyl or PEG pendants per bPEI chain.

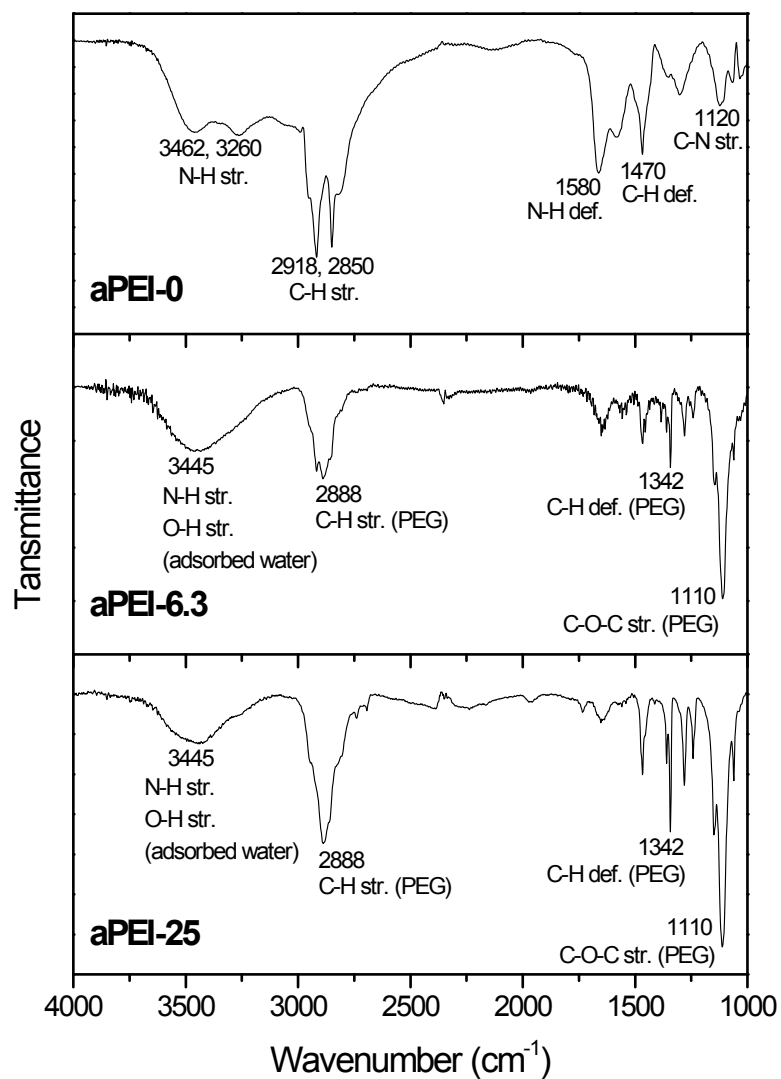


Fig. S1 FT-IR spectra of aPEIs.

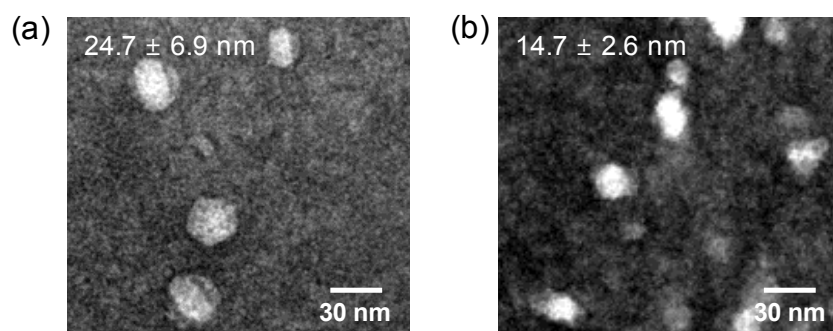


Fig. S2 TEM images of (a) aPEI-0 and (b) aPEI-6.3 NPs. The average particle sizes were indicated.

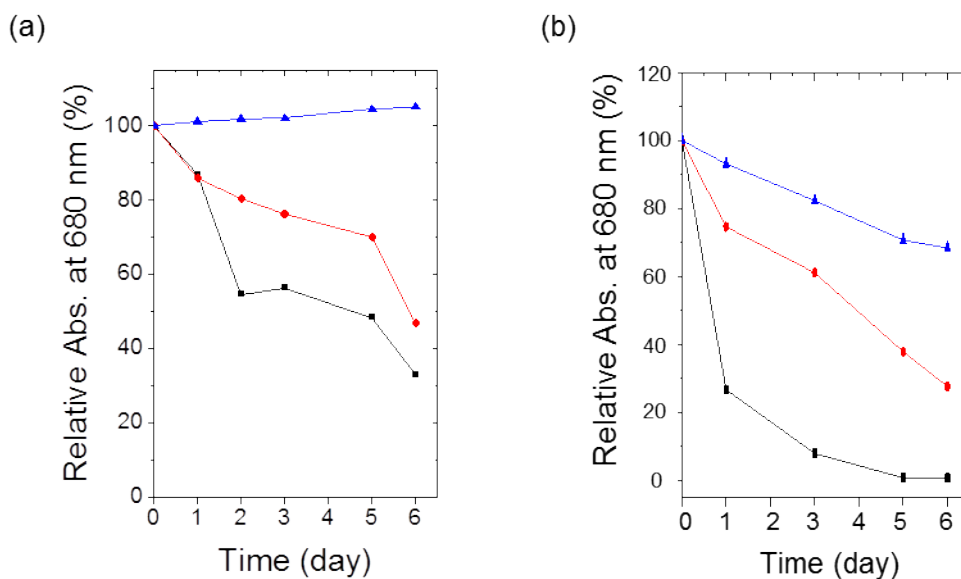


Fig. S3 Temporal absorbance change showing the colloidal stability of aPEI NPs (1 mg mL^{-1} in deionized water (a) and 10% serum at 37°C (b)): (black) aPEI-0, (red) aPEI-6.3, and (blue) aPEI-25. The agglomerates of NPs formed in the course of time were removed with a syringe filter (pore diameter $0.2 \text{ }\mu\text{m}$) prior to every spectral measurement.

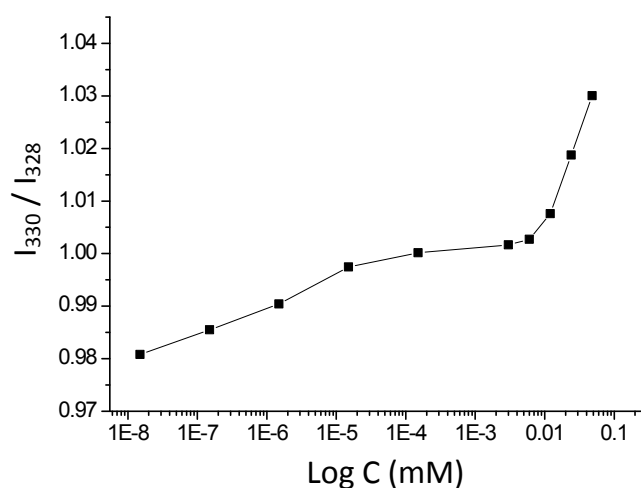


Fig. S4 Critical micelle concentration (CMC) was measured based on the partition change of pyrene between the hydrophobic core and the aqueous environment upon micelle formation. The CMC value of aPEI NPs was estimated as $6.3 \text{ }\mu\text{M}$ by monitoring the intensity ratio of the pyrene excitation bands at 330 and 328 nm (I_{330}/I_{328}) as a function of particle concentration.

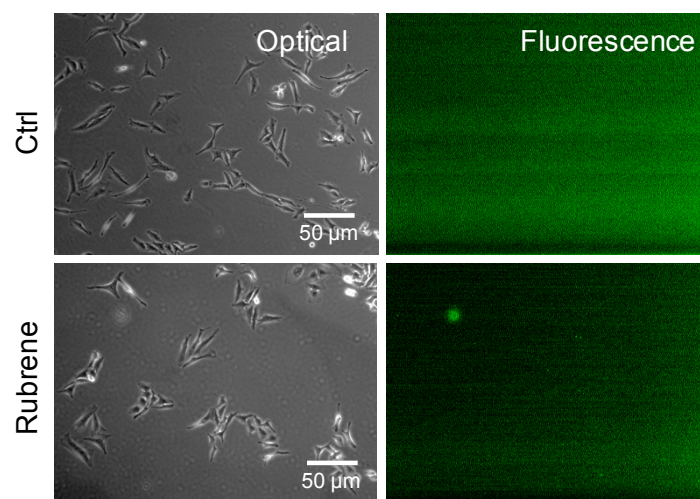


Fig. S5 Optical and fluorescence images of HeLa cells, non-treated (Ctrl) and treated with rubrene for 12 h of incubation.

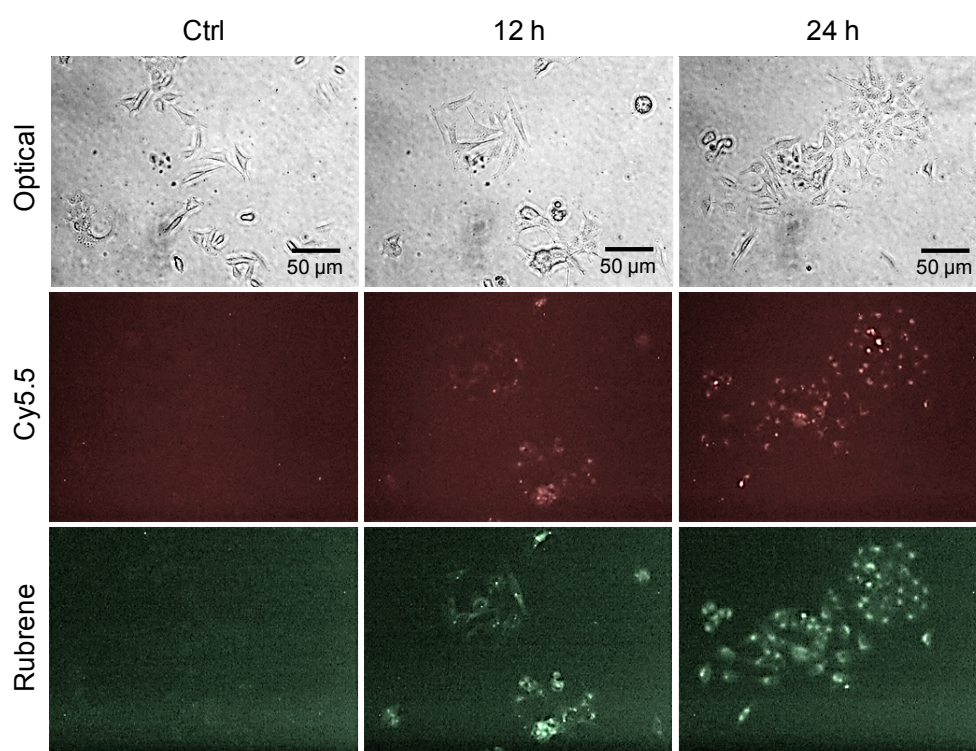


Fig. S6 Optical and fluorescence (Cy5.5 and rubrene channels) images of HeLa cells treated with Cy5.5-labeled aPEI-25 NPs encapsulating rubrene for 12 and 24 h of incubation.

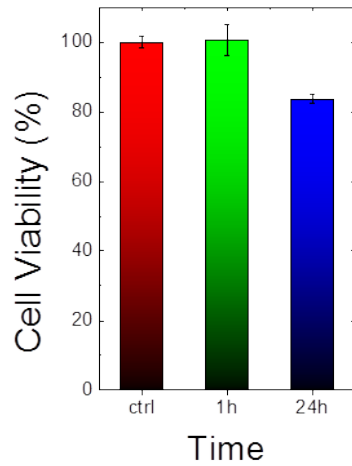


Fig. S7 *In vitro* cytotoxicity of aPEI-25 NPs against HeLa cells, evaluated by the colorimetric MTT assay. Cells were treated with NPs for 1 and 24 h of incubation and assayed in comparison with untreated cells (ctrl).

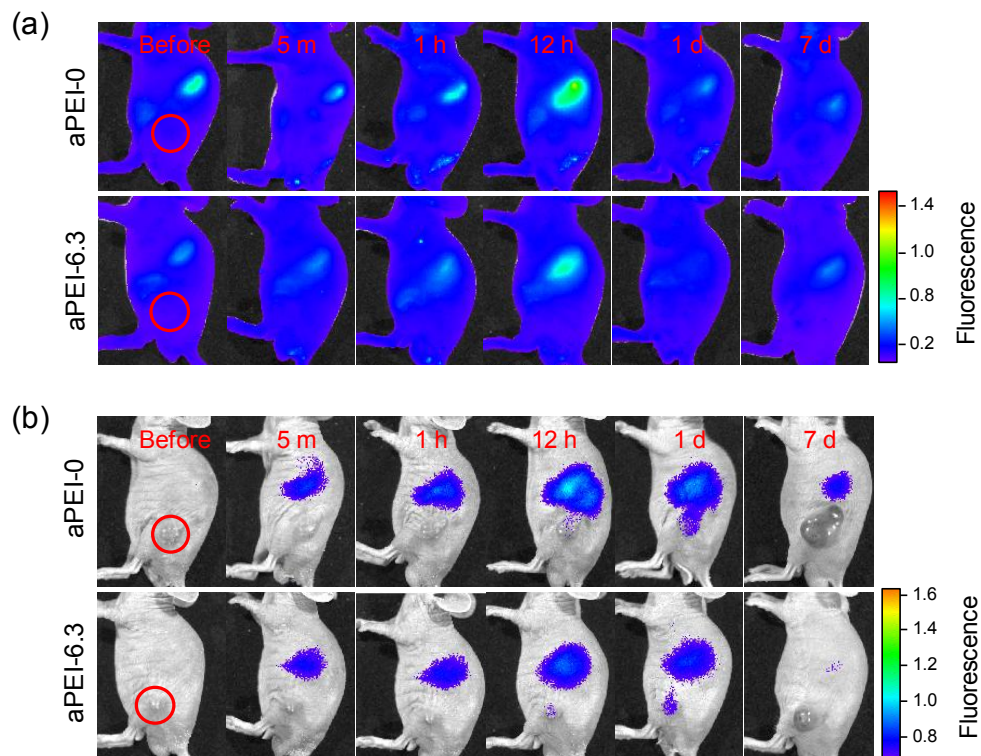


Fig. S8 *In vivo* NIRF images showing the biodistribution of Cy5.5-labeled aPEI-0 and aPEI-6.3 NPs encapsulating IR780, intravenously injected into SCC7 tumor-bearing mice ($n = 5$). 2-Channel NIRF

signals were taken for Cy5.5 (a: $\lambda_{\text{ex}} = 675 \text{ nm}$, $\lambda_{\text{em}} = 720 \text{ nm}$) and IR780 (b: $\lambda_{\text{ex}} = 745 \text{ nm}$, $\lambda_{\text{em}} = 800 \text{ nm}$) channels, at the indicated time points before and after tail vein injection of the NPs. Red circles indicate the tumor location.

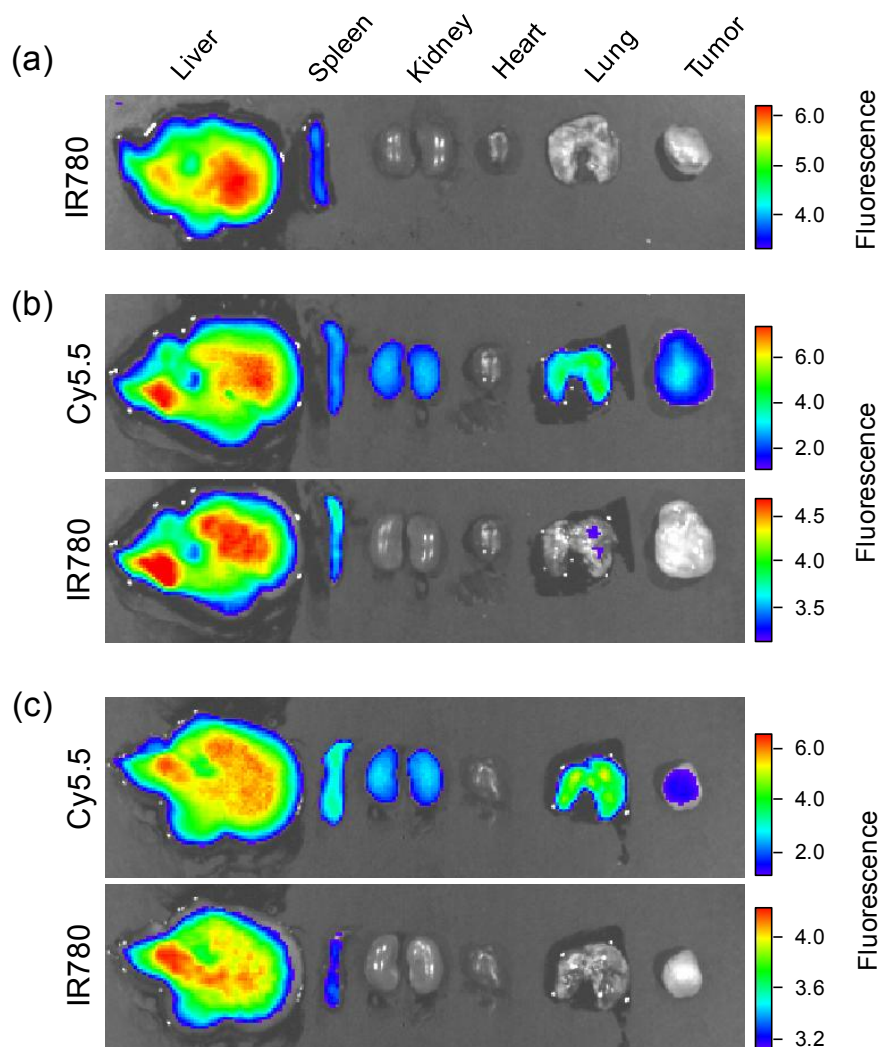


Fig. S9 *Ex vivo* NIRF images showing the biodistribution of free IR780 (a) and IR780 loaded in the Cy5.5-labeled aPEI NPs (b: aPEI-0 NPs and c: aPEI-6.3 NPs) in SCC7 tumor-bearing mice. The organs were collected from the mouse bodies at 7 d post-injection. 2-Channel NIRF signals were taken for Cy5.5 ($\lambda_{\text{ex}} = 675 \text{ nm}$, $\lambda_{\text{em}} = 720 \text{ nm}$) and IR780 ($\lambda_{\text{ex}} = 745 \text{ nm}$, $\lambda_{\text{em}} = 800 \text{ nm}$).

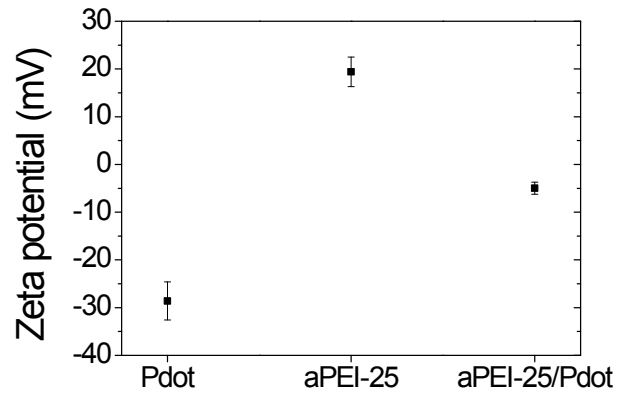


Fig. S10 Zeta potentials of Pdot, aPEI-25 NPs, and Pdot-loaded aPEI-25 NPs (Pdot: aPEI-25 = 1:100 by weight).

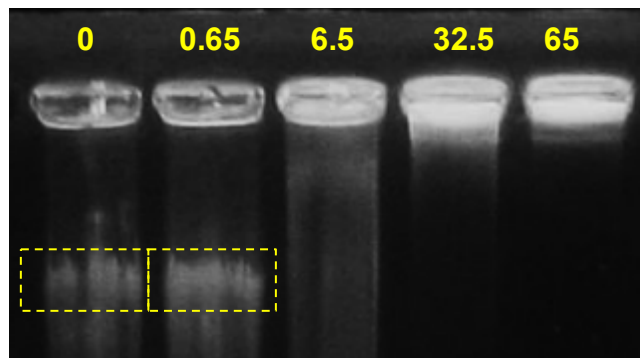


Fig. S11 Gel retardation assay with aPEI-25 NPs/DNA complexes. N/P ratios are indicated for every lane. The squares in the photo indicate free DNA.

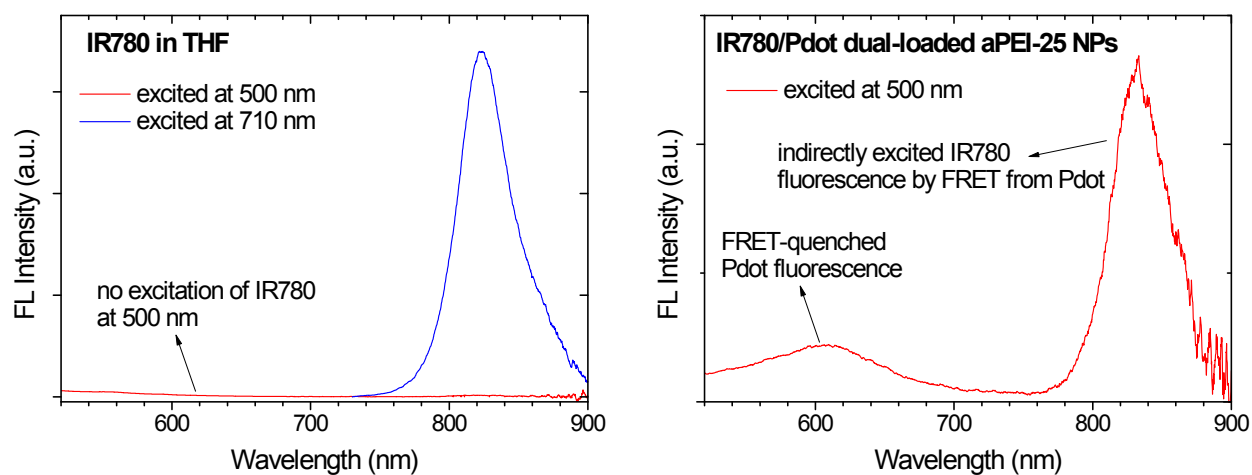


Fig. S12 PL spectra (red: excited at 500 nm, blue; excited at 710 nm) of IR780 solution in THF (left) and water-dispersed aPEI-25 NPs co-loaded with both Pdot and IR780 (right).

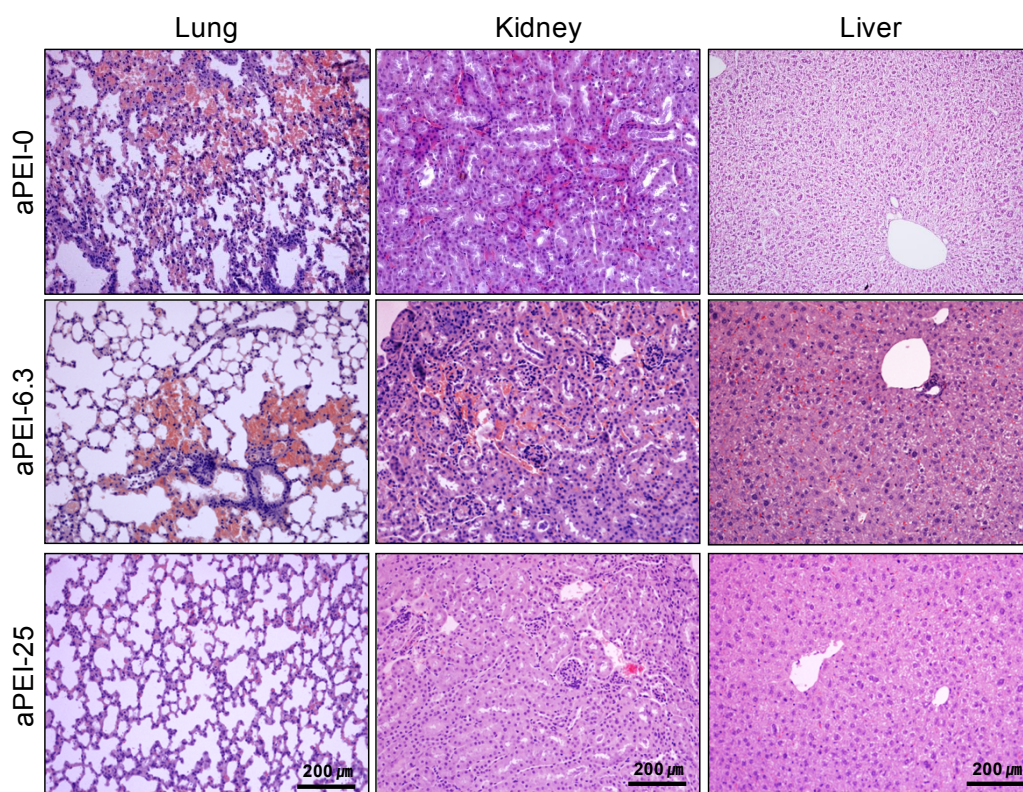


Fig. S13 Representative histological photomicrographs of hematoxylin (H) and eosin (E) stained organ sections resected at 7 d post-injection of aPEI NPs.

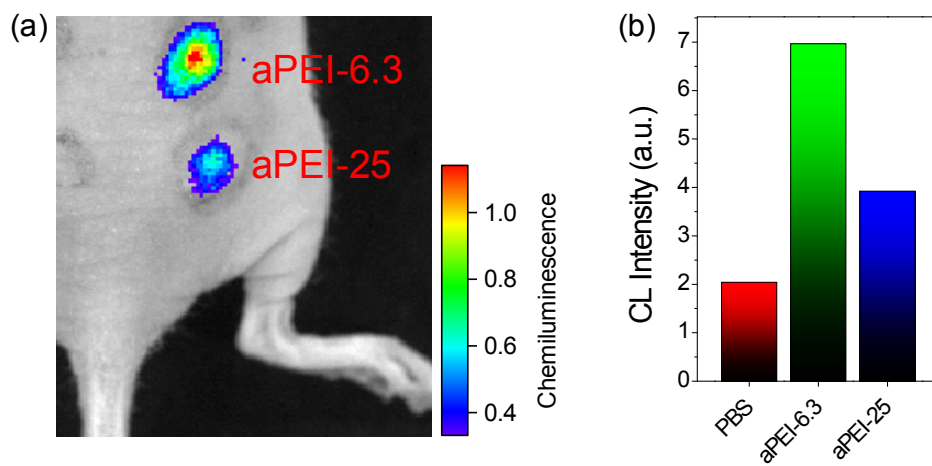


Fig. S14 (a) Inflammation imaging obtained with a H_2O_2 -responsive chemiluminescence (CL) nanoprobe in a mouse that was intradermally injected with aPEI-6.3 and aPEI-25 NPs. (b) Generated CL intensities indicating the degree of inflammation induced by PBS or aPEI NPs.